Materials Research, Vol. 12, No. 1, 57-62, 2009

Phosphorus Emitter and Metal - Grid Optimization for Homogeneous (n^+p) and Double-Diffused ($n^{++}n^+p$) Emitter Silicon Solar Cells

Manuel Cid Sánchez*, Nair Stem

Departamento de Engenharia de Sistemas Eletrônicos,
Escola Politécnica, Universidade de São Paulo – USP,
Av. Prof. Luciano Gualberto, Travessa 3, 158,
05508-970 São Paulo - SP, Brazil

Received: May 19, 2008; Revised: February 5, 2009

This work focuses on studying two types of structure: homogeneous and double-diffused emitter silicon solar cells. The emitter collection efficiencies and the recombination current densities were studied for a wide range of surface dopant concentrations and thicknesses. The frontal metal-grid was optimized for each emitter, considering the dependence on the metal-semiconductor contact resistivity and on the emitter sheet resistance. The best efficiency for n^+p structures, $\eta \approx 25.5\%$, is found for emitters with thicknesses between (0.5-3) μm and surface doping concentrations in the range 2×10^{19} cm^{-3}– 4×10^{18} cm^{-3}; while the $n^{++}n^+p$ structure a maximum efficiency of $\eta \approx 26.0\%$ was identified for an even wider range of emitter profiles.

Keywords: *modelling, emitter optimization, efficiency limits*

1. Introduction

Solar cell emitters can be divided into two different types: a) homogeneous and b) double-diffused (DD) or selective. The homogeneous emitters are characterized by having the same doping level under passivated and metal-contacted regions, while the DD ones present a higher doping level under the metal-contacted one. The passivated regions can be obtained experimentally by a light phosphorus diffusion. In case of DD emitters, this light diffusion is usually preceded by a heavy diffusion only under the metal-grid region.

The theoretical simulations are quite helpful in the development of fabrication processes of silicon solar cells, allowing defining the requirements for high quality emitters and high efficiency solar cells. In this work a re-optimization aiming to compare double-diffused ($n^{++}n^+$) and homogeneous (n^+) Gaussian profile phosphorus emitters was performed using a one-dimensional model with analytical solutions[1,2], the currently accepted internal parameters[3] and the updated intrinsic concentration, $n_i = 9.65 \times 10^9$ cm^{-3}[4].

Despite a complete theoretical re-optimization for homogeneous emitters having already been made[5], the previous DD (double-diffused) emitter optimizations were carried out using either obsolete parameters[6,7,8], or without considering the light trapping effect and the metal-grid design optimization[9]. Thus, a re-optimization for the double-diffused emitter solar cells ($n^{++}n^+p$) is necessary. In order to establish a direct comparison between DD and homogeneous emitter structures, the latter will also be re-optimized here.

2. Theoretical Modelling Assumptions

The homogeneous emitters have the same N_s and W_e under the passivated and the metal-contacted regions; on the other hand the double-diffused (DD) emitters are characterized by having a higher N_s under the metal-contacted one, with $N_s = 1 \times 10^{20}$ cm^{-3} and $W_e = 2.0$ μm (13 Ω/square) used in this work. The adopted expression for the surface recombination velocity under passivated region, $S_p = N_s \times 10^{-16}$ cm/s, is the one typically found in oxidized surfaces followed by FGA annealing[3], values corroborated by M. Kerr et. al.[10]. While under metal-contacted regions a constant $S_p = 3 \times 10^6$ cm/s, was used.

In order to better show the emitter limitations, a 1 Ω.cm resistivity p-type base region with 300 μm thickness, a 1.5 ms minority carrier lifetime and a zero rear surface recombination velocity was assumed. In sequence, the electrical output parameters (J_{sc}, V_{oc}, FF and η) of n^+p and $n^{++}n^+p$ complete structures were studied. The short-circuit current density, J_{sc} was calculated taking into account the light trapping effect and the AM1.5G spectrum (ASTM G173-03). The open-circuit voltage, V_{oc} was determined as a function of total emitter recombination, J_{oe}, the base recombination and J_{sc}. The relation between the fill factor, FF and the device series resistance was expressed as function of the optimized total resistive power loss, p_{tot} and the intrinsic fill factor, FF_o [11], as defined in the expression:

$$FF = FF_O(1 - p_{tot}) \quad (1)$$

3. Upgraded Program

In order to produce contour plots assuring accuracy even for thicker and highly doped emitters for the range $N_s = 1 \times 10^{18}$ cm^{-3} – 1×10^{20} cm^{-3} and W_e = (0.1 to 10) μm, the 10th order approximation was adopted to fulfill the optimizations.

As a matter of fact, the 5th order approximation, used to calculate with accuracy the emitters with thicknesses up to 5 μm at the previous work[9], became unsatisfactory for higher values of thicknesses (required at this work).

Since the emitter can be divided into two different regions: passivated and metal-contact and the surface doping concentration was kept constant under the latter one, the accuracy on the recombination under the passivated region was chosen to be analyzed.

For instance, a 10 μm thickness emitter with $N_s = 1 \times 10^{20}$ cm^{-3} presented $J_{oepass} = 158$ fA.cm^{-2} as the recombination current density under the passivated region (without the metal-contact factor, F_m) using the 10th order approximation, being about 5% inferior than the solution obtained by the PC1D code. On the other hand, if a 3rd and a 5th order approximations were considered these errors would increase up to 39.2 and 26.5%, respectively.

*e-mail: mcid@lme.usp.br

4. Metal-Grid Optimization

In the present work, Ti-Pd-Ag metal-grid designs, typical of laboratory solar cell with 2 x 2 cm area, are optimized using classical models[5,11]. This optimization is performed by an iterative method until the shadowing loss becomes equal to the total resistive power loss, p_{tot} (emitter layer, metal fingers and metal contacts) for each emitter. The metal (Ti) – semiconductor (Si) contact resistances were calculated taking into account their dependence on the emitter[5,12] and Ag contact resistance was considered to be $\approx 2 \times 10^{-6}\ \Omega.cm^2$ [13]. The initial finger width was D = 6 μm and after being electroplated, D_F = 30 μm, with a 10 μm thickness. The bus-bar was supposed to be tapered and with a two-step Ag plating, typical of high efficiency solar cells[14].

The shadowing factor, F_s was extracted from the total shadowing power losses (fingers, p_{sf} plus bus-bar, p_{sb}). However, the metal-contacted factor, F_m, due to the area increase caused by the electroplating, is a fraction of the p_{sf} (20%) and p_{sb} (50%), as presented in expression (2).

$$F_m = 100 \times \left((D / D_F) \times p_{sf} + 0.5 \times p_{sb} \right) \quad (2)$$

Figures 1 and 2 show the optimized shadowing factors, F_s and the spacing between fingers, S as functions of N_s and W_e for single and double emitters.

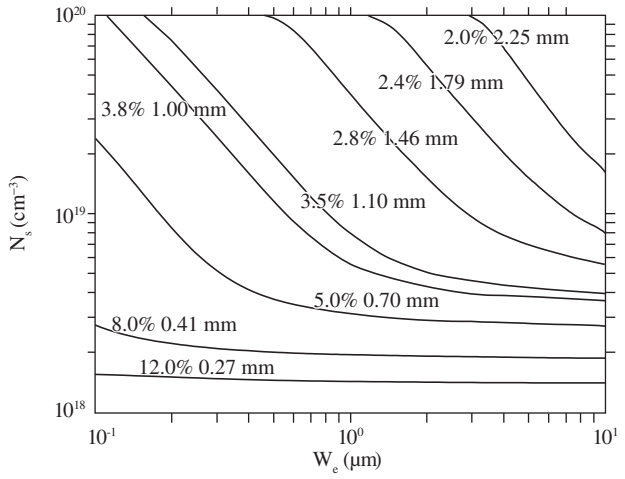

Figure 1. Optimum shadowing factors, F_s (%) and spacing between fingers, S (mm) as functions of surface doped concentration, N_s and thickness, W_e for homogeneous emitters.

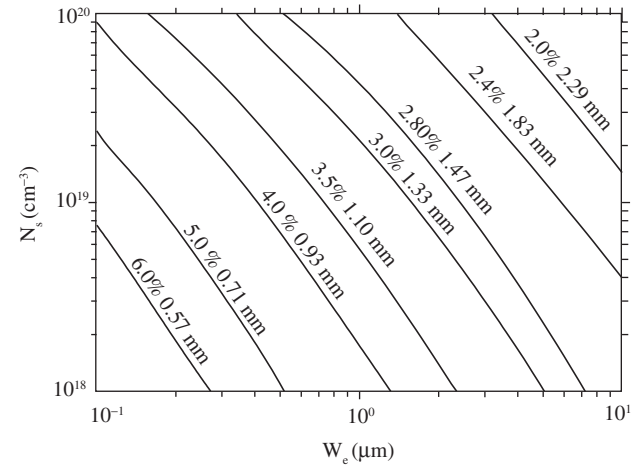

Figure 2. Optimum shadowing factors, F_s (%) and spacing between fingers, S (mm) as functions of surface doped concentration, N_s and thickness, W_e for DD emitters.

Comparing these figures, it can be observed that the higher the surface doping concentration (>2 x $10^{19} cm^{-3}$) of thick emitters (>3 μm), the higher the required spacing between fingers (>1.79 mm), and consequently, the lower F_s (about 2.4-2%) for both types of emitters. Nevertheless, for lowly doped emitters (1 x 10^{18} cm^{-3} < N_s < 4 x 10^{18} cm^{-3}) a significantly different behavior can be observed. While the F_s and S contour plots of homogenous emitters present a plateau as the thickness increases, the DD plots decrease continuously. This difference in behavior is due to the higher metal-contact resistance of homogeneous emitters, making a higher F_s necessary; and therefore, a lower S.

5. Emitter Optimization

The emitters had their collection efficiency, η_c and their recombination current density components under metal-contacted, J_{oemet}, and passivated, J_{oepass}, regions calculated as function of N_s and W_e. The total emitter recombination current densities, J_{oe} result from the sum of the components J_{oemet} and J_{oepass} multiplied by their respective optimized weight factors, (F_m) and (1-F_m), as commented in the following.

According to the modelling results the Gaussian profile emitters can provide high collection efficiencies ($\eta_c \geq 98\%$). Moreover, in order to maintain a high η_c as the thickness increases, a steady decrease in the surface doping concentration is imperative. Thus, emitters with N_s = 2 x 10^{19} cm^{-3}, 1 x 10^{19} cm^{-3}, 4 x 10^{18} cm^{-3} and 2 x 10^{18} cm^{-3} require W_e = (0.94, 1.73, 3.68 and 6.17) μm, respectively to provide the same η_c = 98%.

5.1. Homogeneous emitter recombination (n^+)

The emitter recombination current densities under both metal-contacted, J_{oemet} and passivated, J_{oepass} regions are shown in Figure 3 and Figure 4, respectively. In Figure 3, it can be observed that the moderately doped emitters, 4 x 10^{18} cm^{-3} < N_s < 2 x 10^{19} cm^{-3} with thickness in the range, 0.5 μm < W_e < 3 μm have J_{oemet} between $\approx 3.6 \times 10^3$ $fA.cm^{-2}$ and $\approx 3.3 \times 10^2$ $fA.cm^{-2}$. In contraposition, Figure 4 shows that the passivated recombination component in the same region, J_{oepass} is much lower, between ≈11 $fA.cm^{-2}$ and ≈88 $fA.cm^{-2}$. Despite this difference, sometimes the determining contributor to the total J_{oe} is the passivated region, J_{oepass}, since these components must be also multiplied by the corresponding area weight factors.

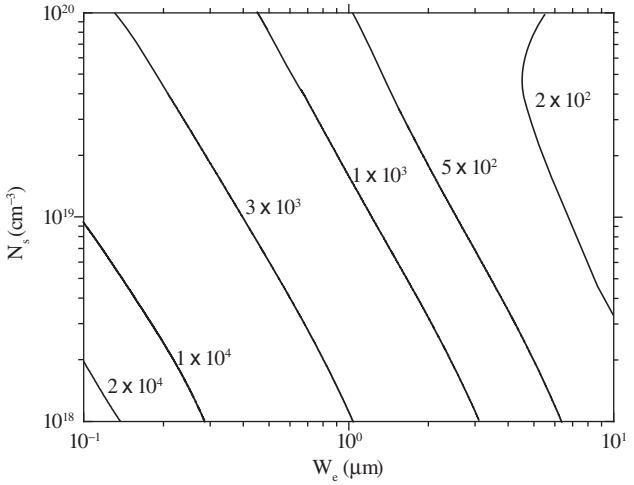

Figure 3. Metal-contacted recombination current density, J_{oemet} ($fA.cm^{-2}$) vs. surface doping concentration, N_s and thickness, W_e, under homogeneous emitters ($S_p = 3 \times 10^6$ cm/s).

5.2. Double-diffused emitters recombination ($n^{++}n^{+}$)

Differently from the homogeneous emitters, the metal-contacted recombination component of the DD ones is always $J_{oemet} = 315$ fA.cm^{-2}, since it was assumed a fixed $N_s = 1 \times 10^{20}$ cm^{-3} and $W_e = 2$ μm under this region for each studied case. Under the passivated region the component, J_{oepass} is the same shown in Figure 4.

A comparison between the total recombination, J_{oe} for both types of emitters is shown in Figure 5 as function of emitter N_s and W_e. It can be observed that the homogeneous total recombination, in the majority of cases, is higher (30 fA.cm^{-2} < J_{oe} < 200 fA.cm^{-2}) than the DD case (12 fA.cm^{-2} < J_{oe} < 200 fA.cm^{-2}), due to the lower recombination loss under the metal-contacted regions in the latter type of emitters. This difference becomes meaningful mainly for the lowly/moderately doped emitters (1×10^{18} cm^{-3} < N_s < 7×10^{18} cm^{-3}) pratically in the whole thickness range (0.1 μm < W_e < 10 μm), where the DD J_{oe} can reach values between 12 fA.cm^{-2} and 18 fA.cm^{-2}.

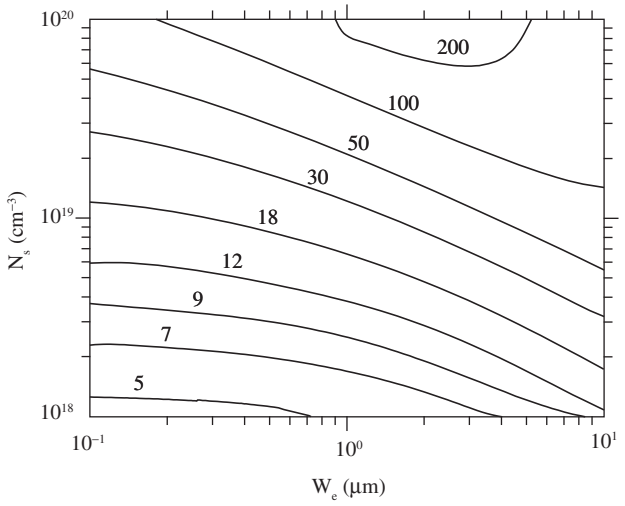

Figure 4. Passivated current density recombination, J_{oepass} (fA.cm^{-2}) as a function of surface doping concentration, N_s and thickness, W_e for both types: homogeneous and DD-emitters ($S_p = N_s \times 10^{-16}$ cm/s).

Another remarkable point in Figure 5 is that the total J_{oe} of both emitter types are practically coincident for moderately doped (5×10^{18} cm^{-3} < N_s < 4×10^{19} cm^{-3}) emitters with thickness range (2 μm < W_e < 10 μm) and also for highly doped ($N_s > 6 \times 10^{19}$ cm^{-3}) emitters with (0.7 μm < W_e < 10 μm), due to a non-significant contribution of the metal-contacted region.

5.3. Emitter recombination for optimum homogeneous and DD structures

A comparison between the emitter recombination current density (including the component contributions and the total J_{oe}) of the optimum emitters from Figures 8 and 11 is presented in Table 1. The optimum homogeneous emitter is $N_s = 7.5 \times 10^{18}$ cm^{-3} with 1.7 μm, while the DD optimum emitter is given by $N_s = 3 \times 10^{18}$ cm^{-3} and $W_e = 1.4$ μm.

Analyzing Table 1, it can be concluded that the passivated region of both types of emitters is the dominant component. The higher J_{oepass} presented by the homogeneous emitter is principally due to the difference between the respective surface doping concentrations, $N_s = 7.5 \times 10^{18}$ cm^{-3} for homogeneous and $N_s = 3 \times 10^{18}$cm^{-3} for DD, since their optimum metal-contacted factors are quite close, the former $F_m \approx 0.88\%$ ($F_s = 3.21\%$ in Figure 1) and the latter $F_m \approx 0.93\%$ ($F_s = 3.49\%$ in Figure 2).

6. Output Electrical Parameters of N⁺P Solar Cells

The output electrical parameters (short-circuit current density, J_{sc}; open-circuit voltage, V_{oc} and efficiencies, η) of homogeneous emitter silicon solar cells are shown in the contour plots of Figures 6, 7 and 8, respectively.

Table 1. Comparison between the homogeneous and DD emitter recombination current density for the optimum complete structures from Figure 8 and 11: the components multiplied by the weight factors, $(F_m).J_{oemet}$ and $(1\text{-}F_m).J_{oepass}$, and the total, J_{oe}.

Type	Fm %	$(F_m).J_{oemet}$ fA.cm^{-2}	$(1\text{-}F_m).J_{oepass}$ fA.cm^{-2}	J_{oe} fA.cm^{-2}
n^+	≈0.88	≈7.4	≈24.5	≈31.9
$n^{++}n^+$	≈0.93	≈2.9	≈11.0	≈13.9

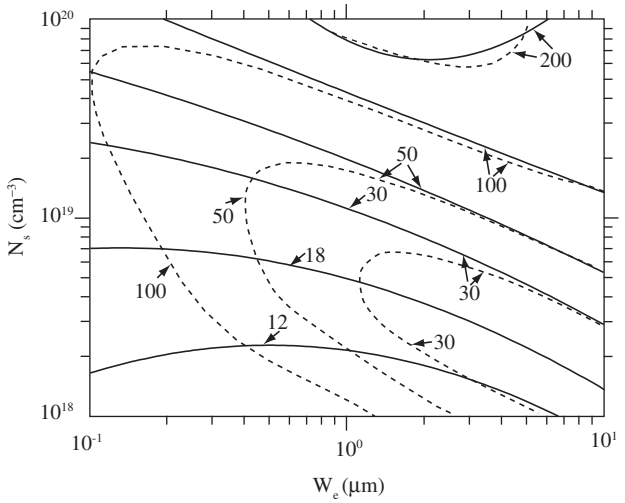

Figure 5. Total emitter recombination, J_{oe} (fA.cm^{-2}) vs. the emitter surface doping concentration, N_s and thickness, W_e. The dashed and continuous lines are for homogeneous and DD emitters, respectively.

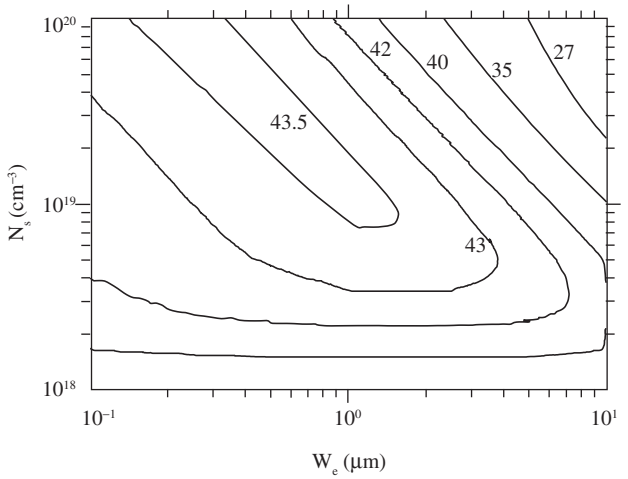

Figure 6. Short-circuit current density contour plots, J_{sc} (mA/cm^2) as a function of surface doping concentration, N_s and thickness, W_e of n⁺p structure solar cell with base resistivity 1 Ω.cm.

According to Figure 6, the short-circuit current densities reach the maximum, J_{sc} = 43.0 mA.cm^{-2} – 43.5 mA.cm^{-2}, for emitters with surface doping concentration 4 x 10^{18} cm^{-3} < N_s < 2 x 10^{19} cm^{-3} and thickness 0.4 μm < W_e < 4.0 μm. However, it can be noticed that high short-circuit current densities can be reached even for highly doped emitters (2 x 10^{19} cm^{-3} – 1 x 10^{20} cm^{-3}) since their thickness are about (0.4-0.6) μm.

In Figure 7, the V_{oc} were calculated as a function of the total J_{oe}, taking into account both components (J_{oepass} and J_{oemet}) and their respective weight factors from the metal-grid optimization, as shown by Figures 1 and 2, and Equation (2).

This figure shows that the maximum open-circuit voltages, V_{oc} are between 700 mV and 715 mV, for emitters with surface doping concentrations N_s < 2 x 10^{19} cm^{-3} and thickness range 0.4 μm < W_e < 10.0 μm, similarly to the bottom right corner of Figure 4. On the other hand, there is a decrease of 30 mV for highly and thin doped emitter N_s = 1 x 10^{20} cm^{-3} and W_e = 0.2 μm, the upper left corner, resulting in efficiencies of about η = 24.3%, as it can be seen in Figure 8.

According to Figure 8, the maximum efficiencies, η = 25.5-25.3%, are obtained in the range N_s = 2 x 10^{19} cm^{-3} - 4 x 10^{18} cm^{-3}. The surface doping concentration upper bound (≈2 x 10^{19} cm^{-3}) allows lower thicknesses (≈0.5 μm < W_e < ≈1 μm); while the lower bound (≈4 x 10^{18} cm^{-3}) requires thicker emitters, ≈1 μm < W_e < ≈3 μm. The output parameters of a solar cell with an intermediate N_s from the optimum range, N_s = 7.5 x 10^{18} cm^{-3} and 1.7 μm (R_{square} ≈ 87.5 Ω/square), are J_{sc} = 43.4 mA.cm^{-2}, V_{oc} = 710.3 mV, FF = 0.826 and η = 25.5% with an optimized metal-grid design given by F_s = 3.21%, F_m = 0.88% and S ≈ 1.24 mm. Thus, in order to mantain a high efficiency there must be a trade off between high short-circuit current density and open-circuit voltage (minimum recombination).

Comparing the results of Figure 8 to the ones obtained in a previous work[9], it can be seen that the maximum efficiencies at that work, η = (21.6-21.7%), were reached for surface doping concentration and thickeness ranges, N_s = (1 x 10^{19} – 5 x 10^{18}) cm^{-3} and W_e = (1.2 – 2.0) μm respectively, also belonging to the optimum ranges of the η = 25.3% contour plot in Figure 8. Nevertheless, the difference between the absolute values of efficiencies is strictly related to the introduction of the light trapping effect in the semiconductor, generating an important increase of the short-circuit current density, changing from 38.6 mA.cm^{-2} to 43.5 mA.cm^{-2}. The open-circuit voltages that were about 690 mV for emitters with surface doping level, N_s = 5 x 10^{18} cm^{-3}, reached the maximum value V_{oc} > 700 mV, as shown in Figure 7. The main cause for the differences between the maximum V_{oc} can be owed to the fact that the previous structures were made of three different regions n$^+$pp$^+$; and therefore, the recombination coming from a p$^+$ region was inserted.

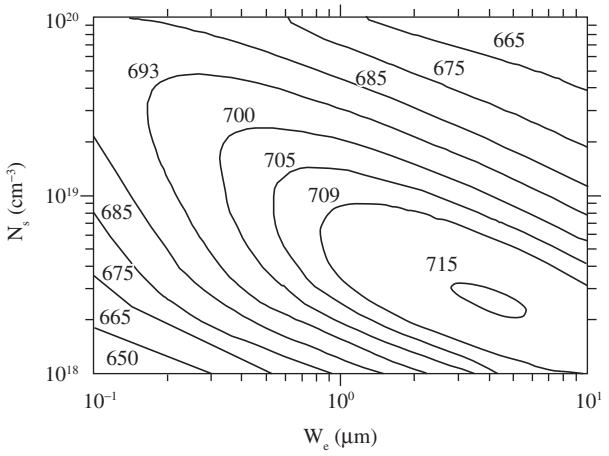

Figure 7. Open-circuit voltage contour plots, V_{oc} (mV) as a function of surface doping concentration, N_s and thickness, W_e of n$^+$p structure solar cell with base resistivity 1 Ω.cm.

7. Output Electrical Parameters of N^{++}N$^+$P Solar Cells

Similarly to the homogeneous emitter solar cells, the output electrical parameters (short-circuit current density, open-circuit voltage and efficiency) of the DD emitter solar cells were analyzed in contour plots, as presented in Figures 9, 10 and 11.

Analyzing that the short-circuit current density, J_{sc} surrounded by the 43.4 mA.cm^{-2} contour plot in Figure 9 present the J_{sc} between 43.4 mA.cm^{-2} < J_{sc} ≤ 43.6 mA.cm^{-2}. On the other hand, in Figure 10, it can be verified high open-circuit voltages V_{oc} = 725 mV for low doped emitters, with N_s < 2 x 10^{18} cm^{-3} in a wide range of thickness, 0.25 μm < W_e < 4.0 μm.

Comparing Figures 7 to 10, it can be concluded that higher open-circuit voltages are reached in the double-diffused emitter silicon solar cells as it was predicted previously in Figure 5.

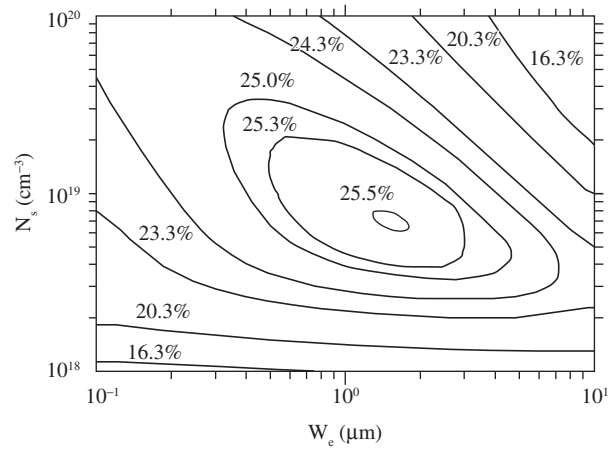

Figure 8. Solar cell efficiency contour plots, η (%) as a function of surface doping concentration, N_s and thickness, W_e of n$^+$p structure solar cell with base resistivity 1 Ω.cm.

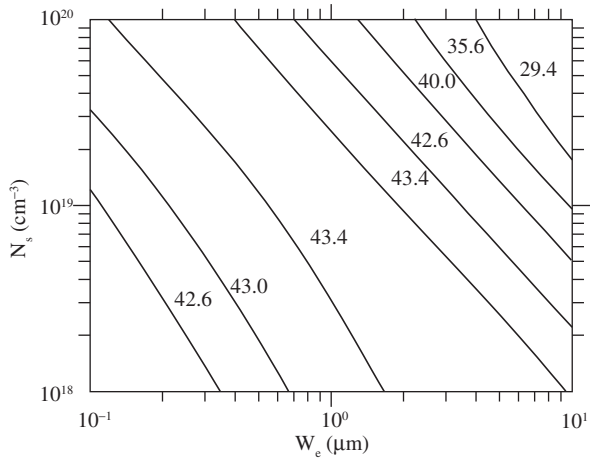

Figure 9. Short-circuit current density contour plots, J_{sc} (mA.cm^{-2}) as a function of surface doping concentration, N_s and thickness, W_e of n^{++}n$^+$p structure solar cell with base resistivity 1 Ω.cm.

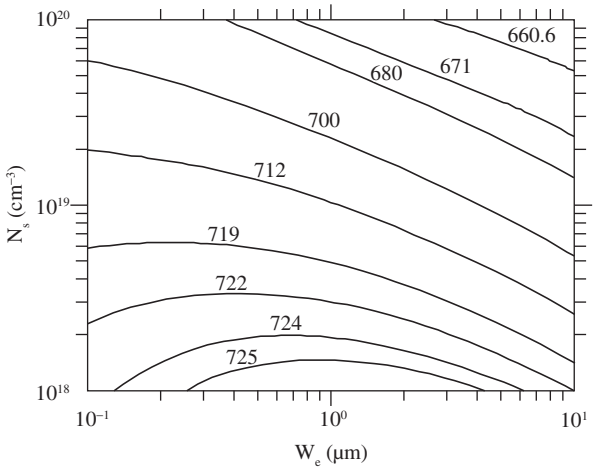

Figure 10. Open-circuit voltage contour plots, V_{oc} (mV) as a function of surface doping concentration, N_s and thickness, W_e of $n^{++}n^{+}p$ structure solar cell with base resistivity 1 Ω.cm.

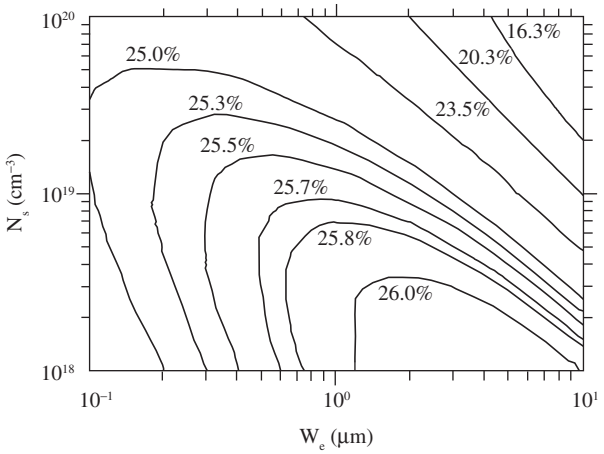

Figure 11. Solar cell efficiency contour plot, η (%) versus the emitter surface doping concentration, N_s and thickness, W_e.

Meanwhile, the $n^{++}n^{+}p$ structures (see Figure 11) can provide higher efficiencies, η = 26.0-25.7% for a wider range of emitter regions, $1 \times 10^{18}\,cm^{-3} < N_s < 1 \times 10^{19}\,cm^{-3}$ with $0.5\,\mu m < W_e < 10\,\mu m$, in agreement with previous results[9]. However, in that work the maximum efficiencies were lower, η = 21.9% (no light trapping) and provided by a narrower range of emitter profiles, $N_s = 1 \times 10^{19}\,cm^{-3} - 5 \times 10^{18}\,cm^{-3}$ and W_e = (1.2-2.0) μm, due to fewer cases having been analyzed ($0.1\,\mu m < W_e < 5\,\mu m$ and $5 \times 10^{18}\,cm^{-3} < N_s < 1 \times 10^{20}\,cm^{-3}$).

For an optimized $n^{++}n^{+}p$ structure with $N_s = 3.0 \times 10^{18}\,cm^{-3}$ and W_e = 1.4 μm (R_{square} = 172.4 Ω/square), the output parameters are J_{sc} = 43.5 mA.cm^{-2}, V_{oc} = 721.5 mV, FF = 0.829 and η = 26.0%. The corresponding optimized metal-grid is defined by F_s = 3.49%, F_m = 0.93% and S = 1.11 mm.

These results are slightly different from those ones found by A. Aberle et al.[8], where the maximum efficiencies η ≈ 27% were provided also for lightly doped emitters $N_s = 5 \times 10^{18}\,cm^{-3} - 1 \times 10^{19}\,cm^{-3}$, but for a lower thickness range W_e = (0.1-0.3) μm. As shown in Figure 11, despite shallow emitters could also provide high efficiencies, the maximum values, η = 26% were obtained for a shifted thickness range, $1\,\mu m < W_e < 10\,\mu m$. This fact is due to the differences between the used input parameters. At that work, the frontal surface recombination velocity was not variable under passivated region as in this work: S_p = 500 cm/s was kept constant for the four studied surface doping concentrations ($N_s = 1 \times 10^{18}\,cm^{-3}$, $5 \times 10^{18}\,cm^{-3}$, $1 \times 10^{19}\,cm^{-3}$, $5 \times 10^{19}\,cm^{-3}$). Meanwhile, the metal-contacted region surface recombination velocity was a bit lower, $S_p = 1 \times 10^{6}$ cm/s. The parameters under the metal-contacted region were $N_s = 5 \times 10^{19}\,cm^{-3}$ and W_e = 2 μm. As it can be noticed, these results overestimated the efficiencies for shallow and moderately doped emitters, since the metal-contact factor F_m was underestimated by fixing it at 3%. On the other hand, E. Demesmaeker[7], by fulfilling grid-optimization, but adopting R. King[3] parameters and a higher surface doping concentration under the metal-contact region $N_s = 1 \times 10^{21}\,cm^{-3}$, obtained more similar results to this work. Despite the lower optimum efficiencies η = 21%, the correspondent ranges of maximum efficiencies were $N_s = 2 \times 10^{18}\,cm^{-3}$ - $1 \times 10^{19}\,cm^{-3}$ and thickness $1\,\mu m < W_e < 10\,\mu m$.

8. Conclusions

Gaussian profile phosphorus emitters were optimized showing high quality, high collection efficiencies (≥98%) and low recombination (minimum J_{oe} for homogeneous and DD are respectively 30 fA.cm^{-2} and 12 fA.cm^{-2}). The total recombination, J_{oe} of lowly doped homogeneous emitters showed to be strongly dependent on the metal-contacted recombination component, J_{oemet} and on the optimized metal-grid designs.

The optimum homogeneous structure efficiencies (η = 25.5-25.3%) were found for surface doping in the range $N_s = 2 \times 10^{19}\,cm^{-3}$ $4 \times 10^{18}\,cm^{-3}$ together with a thickness of $W_e \approx$ (0.5-3) μm. On the other hand, the best DD structures can provide higher efficiencies (η = 26.0-25.7%) for a wider range of emitter profiles, $1 \times 10^{18}\,cm^{-3} < N_s < 1 \times 10^{19}\,cm^{-3}$ and $0.5\,\mu m < W_e < 10\,\mu m$.

Acknowledgements

Nair Stem was supported by CNPq scholarship under process nº 141460/20008.

References

1. Park J, Neugroschel A, Lindholm, F. Systematic Analytical Solutions for Minority Carrier Transport in Semiconductors with Position-dependent Composition with Application to Heavily Doped Silicon. *IEEE Transaction on Electron Devices*. 1986; ED-33(2):240.
2. Bisschop FJ, Verholf LA, Sinke WC. An Analytical Solution for the Collection Efficiency of Solar Cell Emitters with Arbitrary Doping Profile. *IEEE Transaction on Electron Devices*. 1991; ED-37(2):358.
3. Cuevas A, Basore P, Giroult-Matlakowski G, Dubois C. Surface Recombination Velocity of Highly Doped n-type Silicon. *Journal of Applied Physics*. 1996; 80(6):3370.
4. Altermatt PP, Schumacher JO, Cuevas A, Kerr M, Glunz SW, King RR, Heiser G, Schenk A. Numerical Modeling of Highly Doped Silicon: P Emitters Based on Fermi-Dirac Statistics and Self Consistent Material Parameters. *Journal of Applied Physics.* 2002; 92(6):3187.
5. Cuevas A, Russel DA. Co-optimization of the Emitter Region and the Metal-Grid of Silicon Solar Cells. *Progress in Photovoltaics: Research and Applications*. 2000; 8:603.
6. King RR. Studies of Diffused Phosphorus Emitters: Saturation Current, Surface Recombination Velocity, and Quantum Efficiency. *IEEE Transactions on Electron Devices*. 1990; ED-37(2):365.
7. Demesmaeker E. Theoretical and Experimental Study of Advanced Concepts for High Efficiency Crystalline Silicon Solar Cells. [S.L.]: Katholieke Universiteit Leuven; 1993. [PhD Thesis].

8. Aberle A, Warta W, Knobloch J, Voβ B. *21st IEEE Photovoltaic Specialists Conference*; 1990 May 21-25; Kissimmee, FL.
9. Stem N, Cid M. Studies of phosphorus Gaussian profile emitter silicon solar cells. *Materials Research*. 2001; 4(2):143.
10. Kerr M, Schmidt J, Cuevas A. Surface Recombination Velocity of Phosphorus Diffused Silicon Solar Cell Passivated with Plasma Enhanced Chemical Vapor Deposited on Silicon Nitride and Thermal Silicon Oxide. *Journal of Applied Physics*. 2001; 89(7): 3821.
11. Green MA. *Solar cells – Operating principles, Technology and System Applications.* Englewood Cliffs: Prentice Hall Inc.; 1982.
12. Swirhun SE. Characterization of Majority and Minority Carrier Transport in Heavily Doped Silicon. [S.L.]: Stanford University; 1987. [PhD Thesis].
13. Meier DL, Schroder DK. Contact Resistance: its Measurement and Relative Importance to Power Loss in a Solar Cell. *IEEE Transaction on Electron Devices.* 1984; ED-31 (5): 647.
14. Zhao J, Wang A, Altermatt PP, Wenham SR, Green MA. 24% Efficient PERL Silicon Solar Cell: Recent Improvements in High Efficiency Silicon Solar Cell Research. *Solar Energy Materials and Solar Cells.* 1996; 41/42: 87.